AGU PUBLICATIONS

JGR

Journal of Geophysical Research: Solid Earth

RESEARCH ARTICLE
10.1002/2016JB013095

Key Points:
- The first combined study of Cu and Zn isotopic compositions of an intact oceanic crust
- Large variations in Cu and Zn compositions of the altered oceanic crust
- Copper and zinc isotopes are potential tracers of recycled crustal materials in the mantle

Correspondence to:
J. Huang and S.-A. Liu,
jianhuang@ustc.edu.cn;
lsa@cugb.edu.cn

Citation:
Huang, J., S.-A. Liu, Y. Gao, Y. Xiao, and S. Chen (2016), Copper and zinc isotope systematics of altered oceanic crust at IODP Site 1256 in the eastern equatorial Pacific, *J. Geophys. Res. Solid Earth*, *121*, 7086–7100, doi:10.1002/2016JB013095.

Received 13 APR 2016
Accepted 25 SEP 2016
Accepted article online 28 SEP 2016
Published online 12 OCT 2016

Copper and zinc isotope systematics of altered oceanic crust at IODP Site 1256 in the eastern equatorial Pacific

Jian Huang[1], Sheng-Ao Liu[2], Yongjun Gao[3], Yilin Xiao[1], and Sha Chen[1]

[1]CAS Key Laboratory of Crust-Mantle Materials and Environments, School of Earth and Space Sciences, University of Science and Technology of China, Hefei, China, [2]State Key Laboratory of Geological Processes and Mineral Resources, China University of Geosciences, Beijing, China, [3]Department of Earth and Atmospheric Sciences, University of Houston, Houston, Texas, USA

Abstract This paper presents the first combined Cu and Zn isotopic study of altered oceanic crust at Integrated Ocean Drilling Program (IODP) Hole 1256D that penetrates a volcanic section, a lava-dyke transition zone, a sheeted dyke complex, and a plutonic complex. In the volcanic section, all but one rocks have Cu and Zn isotopic compositions similar to fresh mid-ocean ridge basalt (MORB), reflecting restricted seawater circulation and low oxygen fugacity. Rocks in the transition zone have MORB-like δ^{65}Cu and δ^{66}Zn, indicating the dominant influence of basalt-derived Cu and Zn during alteration. Rocks in the dyke complex have more variable δ^{65}Cu (−0.50–0.90‰) and δ^{66}Zn (0.19–0.55‰) and those in the plutonic complex have δ^{65}Cu of −0.43 to 0.20‰ and δ^{66}Zn of 0.21 to 0.41‰. The rocks with heavier δ^{66}Zn and heavier or lighter δ^{65}Cu relative to MORB are characterized by Cu-Zn depletions, low Li/Yb (<1.0) and low δ^{18}O (<5‰), suggesting that hydrothermal extraction during high temperature alteration of oceanic crust can result in significant Cu and Zn isotope fractionation. Such large Cu and Zn isotopic variations are the results of redox transformation of Cu as well as Cu and Zn isotope fractionation between altered basaltic rocks and dissolved Cu and Zn species in hydrothermal fluids (e.g., $[CuCl_3]^{1-}$, $Zn(HS)_4^{2-}$). This work is the first to define the distribution of Cu and Zn isotopes in an intact oceanic crust with concentration-weighted averages of δ^{65}Cu (0.05 ± 0.03‰) and δ^{66}Zn (0.27 ± 0.01‰). The potential implications of these new observations are discussed.

1. Introduction

Alteration of oceanic crust by seawater plays an important role in controlling global fluxes of elements, and recycling of altered oceanic crust (AOC) in subduction zones provides a means for chemical interaction between the hydrosphere, island arc magmatic systems, and the Earth's mantle [*Staudigel et al.*, 1995]. Metalloid and metal isotope analyses have revealed complex hydrothermal processes, primary mineral dissolution, secondary mineral precipitation, element fluxes, and redox reactions during oceanic crust alteration, which are associated with resolvable fractionation of C-O-S-Li-Fe isotopes [e.g., *Hart et al.*, 1999; *Furnes et al.*, 2001; *Chan et al.*, 2002; *Rouxel et al.*, 2003; *Gao et al.*, 2012] but limited fractionation of Mg [*Huang et al.*, 2015a] and V isotopes [*Prytulak et al.*, 2013].

Copper and Zn are the first-row transition metal elements with two (^{63}Cu, ^{65}Cu) and five (^{64}Zn, ^{66}Zn, ^{67}Zn, ^{68}Zn, ^{70}Zn) stable isotopes, respectively [*Lodders*, 2003]. The potential mechanisms that may fractionate Cu and Zn isotopes during hydrothermal processes include redox reactions (only for Cu isotopes) [e.g., *Rouxel et al.*, 2004; *Markl et al.*, 2006], mineral dissolution and precipitation [e.g., *Rouxel et al.*, 2004; *Mathur et al.*, 2005; *John et al.*, 2008; *Kimball et al.*, 2009; *Li et al.*, 2010; *Mathur and Fantle*, 2015], sorption onto clay minerals or Fe-Mn (hydr)oxides [e.g., *Maréchal et al.*, 2000; *Balistrieri et al.*, 2008; *Little et al.*, 2014a; *Li et al.*, 2015], complexation by organic compounds [e.g., *Bigalke et al.*, 2010], and equilibrium fractionation between different Cu and Zn species [e.g., *Black et al.*, 2011: Fujii *et al.*, 2013; *Pons et al.*, 2011; *Dekov et al.*, 2013]. Measurements of Cu and Zn isotopes in ancient and active hydrothermal systems have uncovered large variations in δ^{65}Cu (−17.0 to 10.0‰) and δ^{66}Zn (−0.43 to 1.33‰) values of hydrothermal fluids and sulfide minerals that precipitated from such fluids [e.g., *Rouxel et al.*, 2004; *Mathur et al.*, 2005, 2009, 2012; *Mason et al.*, 2005; *Wilkinson et al.*, 2005; *Markl et al.*, 2006; *John et al.*, 2008; *Kim et al.*, 2014]. Precipitation of isotopically light Zn sulfide (e.g., sphalerite) at relatively low temperatures (<250°C) might be the primary factor causing the observed δ^{66}Zn variations [*Wilkinson et al.*, 2005; *John et al.*, 2008], and the highly variable

δ^{65}Cu values have been attributed to Cu isotope fractionation during redox reactions, between dissolved Cu species and minerals in hydrothermal systems [*Rouxel et al*., 2004; *Markl et al*., 2006].

Copper is a chalcophile element and mainly hosted by easily altered sulfide phases [e.g., *Doe*, 1994; *Fellows and Canil*, 2012], whereas Zn is more lithophile over chalcophile and hosted by not only sulfide phases but also other minerals (e.g., spinel, olivine, and pyroxene). In addition, Cu is a redox-sensitive element with three oxidation states (0, +1, +2), while Zn is a monovalent element (+2) in natural systems. As redox changes can significantly fractionate Cu but not Zn isotopes, these differences may result in different behavior of Cu and Zn isotopes during oceanic crust alteration that happens under conditions of variable oxygen fugacity and involves mineral dissolution and precipitation [e.g., *Wilson et al*., 2006; *Alt et al*., 2010; *Dziony et al*., 2014]. Study of abyssal peridotite has shown that seafloor alteration at different settings can result in different magnitude and direction of Zn isotope fractionation [*Savage et al*., 2013]. Previous studies show that submarine seawater-derived hydrothermal fluids are enriched in Cu and Zn relative to seawater [e.g., *Campbell et al*., 1988a, 1988b]. This is interpreted as being caused by leaching of Cu and Zn from the AOC during high-*T* hydrothermal alteration due to high solubility of both metals at temperatures of $>$350°C [*Seewald and Seyfried*, 1990]. Measurements of altered rocks from oceanic and ophiolitic sections further suggest that Cu and Zn losses irregularly occur in the dyke and plutonic complexes [e.g., *Alt et al*., 2010 and references therein]. Thus, large Cu and Zn isotope fractionation might be expected during oceanic crust alteration, especially at high temperatures.

Knowledge of Cu and Zn isotopic compositions of the AOC offers the potential to enhance our understanding of the Earth's mantle Cu and Zn isotopic heterogeneity and facilitate the use of Cu and Zn isotopes as tracers of recycled crustal materials. Orogenic and mantle peridotites can display large variations in Cu isotopic compositions, with δ^{65}Cu from $-$0.64‰ to 1.82‰ [*Liu et al*., 2015; *Savage et al*., 2014, 2015]. Based on the light rare earth element (LREE) enrichment features of these samples, such large Cu isotope variations have been attributed to mantle metasomatism by melts/fluids derived from the subducted AOC. This mechanism was also applied to explain variable Cu isotopic compositions observed in some arc and continental basalts [*Liu et al*., 2015]. However, as the Cu isotopic composition of the AOC is, so far, unknown, these explanations are speculative.

To investigate the downhole variations in Cu and Zn isotopic compositions of an intact oceanic crust and the behavior of Cu and Zn isotopes during oceanic crust alteration, we here present the first combined Cu and Zn isotope analyses on altered oceanic crustal rocks recovered from IODP Site 1256 at the East Pacific Rise (EPR). Our results show (1) that low-*T* hydrothermal alteration results in limited Cu and Zn isotope fractionation in the AOC, while significant Cu and Zn isotope fractionation occurred during high-*T* hydrothermal alteration; (2) that the bulk AOC at Site 1256 has mantle-like concentration-weighted average Cu and Zn isotopic compositions.

2. Geological Background and Sample Descriptions

Integrated ODP Site 1256 (6°44.2′N, 91°56.1′W) is situated in the Guatemala Basin on the Cocos plate at the eastern flank of the EPR (Figure 1). The oceanic crust at this site formed ~15 Ma ago during an episode of superfast ocean ridge spreading (~220 mm/yr) [*Wilson et al*., 2006]. The 1271.6 m of drilled crustal rocks were recovered at Site 1256 after penetrating ~250 m of sediments [*Wilson et al*., 2006; *Teagle et al*., 2006, 2012] (Figure 2). As revealed by preliminary downhole stratigraphy established from shipboard core observations and wire line log interpretations onboard [*Wilson et al*., 2003, 2006; *Teagle et al*., 2006], the drilled oceanic crust, from top to bottom, consists of (1) the volcanic section (~250–1004.2 m below seafloor, bsf); (2) the lava-dyke transition zone (1004.2–1060.9 m bsf); (3) the sheeted dyke complex (1060.9–1406.6 m bsf); and (4) the plutonic complex (1406.6–1521.3 m bsf).

The volcanic section comprises ponded lavas, inflated flows, sheet flows, and massive flows. The lava-dyke transition zone, composed of sheet and massive flows, represents a mixing zone between the upwelling hydrothermal fluids and downwelling seawater [*Alt et al*., 2010]. The sheeted dyke complex consists of aphyric basalt intruded by vertical dykes. The lowermost dykes (1348.3–1406.6 m bsf) are partially to completely recrystallized to distinctive granoblastic textures and granulite assemblages [*Koepke et al*., 2008; *Alt et al*., 2010]. The plutonic complex contains a 52 m thick upper gabbro and a 24 m thick lower gabbro separated by two granoblastically recrystallized dyke screens [e.g., *Harris et al*., 2015].

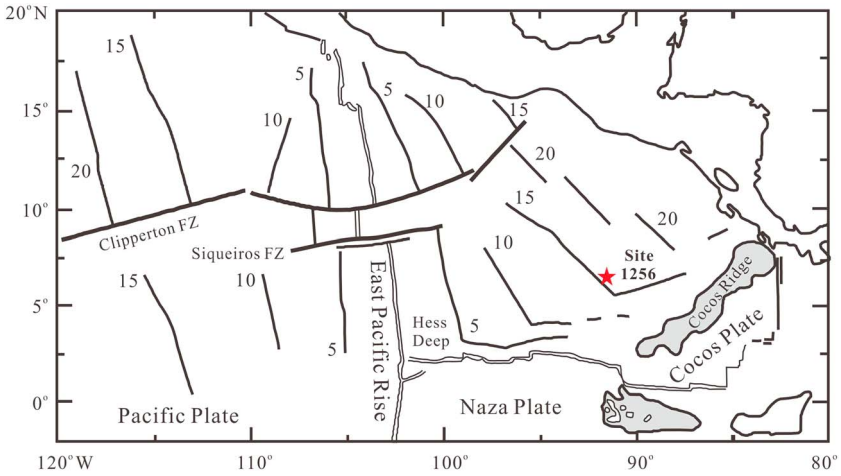

Figure 1. Location of IODP Site 1256 at the Cocos Plate in the eastern Pacific (modified after *Gao et al.* [2012]). Isochrons at 5 Ma intervals are indicated.

The degree of hydrothermal alteration generally increases with increasing depth as manifested by downhole increase of alteration temperatures (Figure 2a). Temperatures of hydrothermal mineral formation, obtained from oxygen isotope measurements of saponite, celadonite, anhydrite, and quartz, range between ~50 and ~135°C in the volcanic section (Figures 2a and 2b). The presence of chlorite, albite, and actinolite indicates that the lava-dyke transition zone was subjected to greenshcist facies metamorphism with alteration temperatures of ~130–180°C (Figure 2a) [*Teagle et al.*, 2006; *Alt et al.*, 2010]. Within the sheeted dyke complex, an early stage of hydrothermal alteration at ~400–850°C is indicated by whole-rock depletions of Cu and Zn (Figures 3a and 3b) and the presence of secondary minerals in rocks and veins, including pyroxene, plagioclase, amphibole, chlorite, epidoite, titanite, and pyrite [*Alt et al.*, 2010]. Subsequent contact metamorphism caused by intrusion of gabbro bodies at ~850–950°C has resulted in granoblastic textures in the lowermost dykes [*Koepke et al.*, 2008; *Alt et al.*, 2010]. The plutonic complex experienced metamorphic

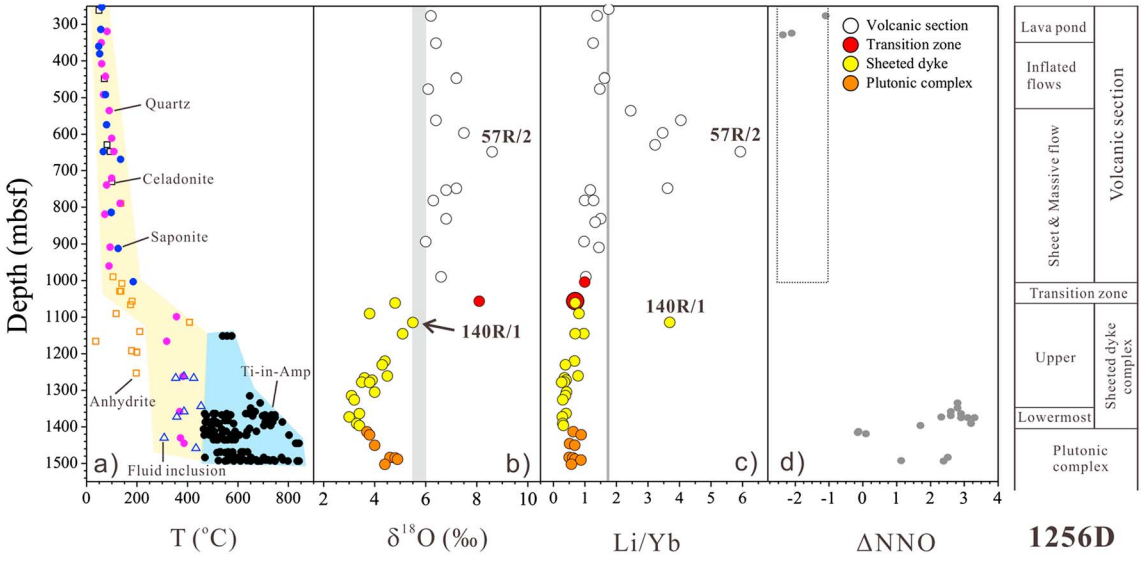

Figure 2. Downhole variations of (a) alteration temperatures, (b) $\delta^{18}O$, (c) Li/Yb, and (d) oxygen fugacity through the oceanic crust at IODP Site 1256. Alteration temperatures were estimated from experimentally determined secondary mineral-water oxygen isotope fractionation factors, fluid inclusions, and Ti-in-amphibole (Amp) geothermometry [*Alt et al.*, 2010]. Anhydrites outside the trend (light yellow empty squares) record either disequilibrium temperatures of precipitation or precipitation during collapse and cooling of the system. Oxygen fugacity (ΔNNO) was calculated using magnetite-ilmenite thermo-oxybarometry [*Koepke et al.*, 2008; *Dziony et al.*, 2014]. The dashed rectangle illustrates similar oxygen fugacity in the volcanic section [*Wilson et al.*, 2006]. The gray bar and line denote the average $\delta^{18}O$ and Li/Yb of MORB, respectively [*Harmon and Hoefs*, 1995; *Gao et al.*, 2012]. The data for $\delta^{18}O$ and Li/Yb are taken from Table 1. (For interpretation of the references to color in this figure legend, the reader is referred to the web version of this article).

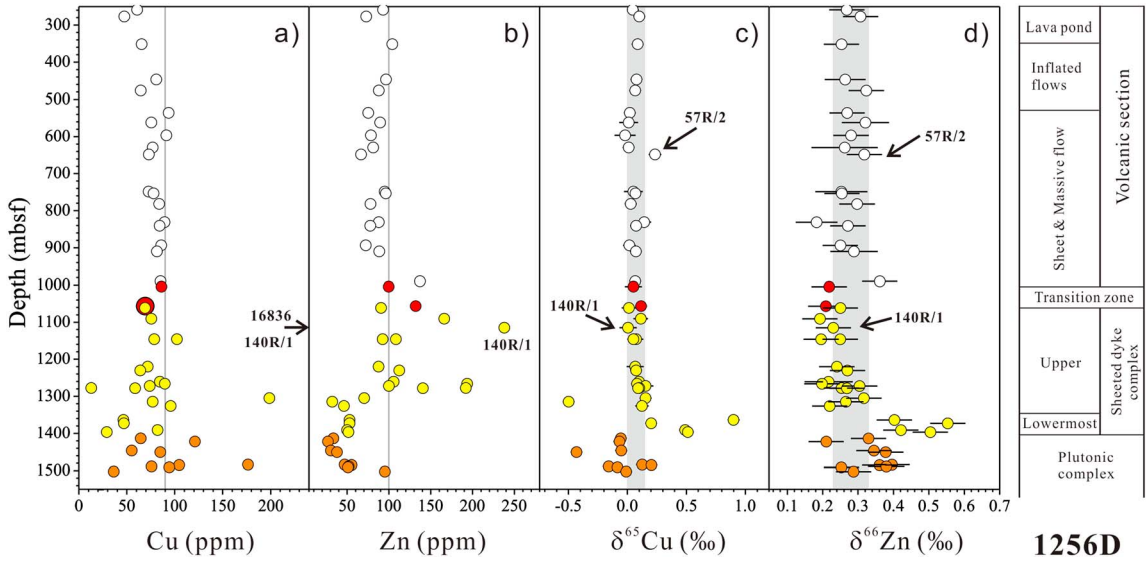

Figure 3. Profiles of (a, b) Cu and Zn concentrations and (c, d) isotopic compositions through the oceanic crust at IODP Site 1256. Reference Cu and Zn concentrations (gray lines) for MORB are 90 ppm and 100 ppm, respectively [*Le Roux et al*., 2010; *Fellows and Canil*, 2012]. Gray bars denote the range of δ^{65}Cu (0.07 ± 0.06‰) [*Liu et al*., 2015; *Savage et al*., 2015] and δ^{66}Zn (0.28 ± 0.05‰) [*Chen et al*., 2013] of MORB. Symbols are the same as those in Figure 2, and the data are taken from Table 1. (For interpretation of the references to color in this figure legend, the reader is referred to the Web version of this article).

conditions (i.e., early amphibolite to later greenshcist facies) similar to those in the lower dykes [*Alt et al*., 2010]. The presence of prehnite, laumontite, and calcite in the plutonic complex further reflects decreasing alteration temperatures and more evolved hydrothermal fluids at the late stage [*Alt et al*., 2010]. Downhole increase of alteration temperatures is clearly reflected by whole-rock δ^{18}O data in rocks from Hole 1256D (Figure 2b) [*Gao et al*., 2012]. Downhole variations in Li-Sr isotopic compositions and Li/Yb ratios (Figure 2c) reveal channelized hydrothermal fluid activity during the accretion and evolution of the oceanic crust at Site 1256 [*Gao et al*., 2012; *Harris et al*., 2015]. High oxygen fugacity (fO_2, ΔNNO up to 3.3) (Figure 2d) records the late-stage oxidation during hydrothermal alteration in the lowermost granoblastic dyke and the plutonic complex [*Koepke et al*., 2008; *Dziony et al*., 2014].

Forty-nine samples from Site 1256, including 39 basalts, 6 gabbros, 2 gabbronorite, 1 breccia, and 1 dolerite were analyzed for Cu and Zn isotopic compositions. These samples represent all the rock types present in the core, cover six sections of the drilled oceanic crust, and span a broad range in depths from 258.5 to 1502.7 m bsf (Figure 2). They have variable Cu and Zn contents ranging from 13.0 to 199 ppm and 27.1 to 193 ppm, respectively, except for the breccia containing much higher contents of Cu (16836 ppm) and Zn (234 ppm) (Figures 3a and 3b). The studied samples have δ^{18}O ranging from 3.0‰ to 8.6‰ [*Gao et al*., 2012] (Figure 2b).

3. Analytical Methods

The detailed procedures for sample digestion, column chemistry, and instrumental analysis are reported in previous studies [*Liu et al*., 2014a, 2014b; *Lv et al*., 2016]. Only a brief description is given below.

3.1. Sample Dissolution and Chemical Purification

Between 6 and 52 mg whole-rock powder samples were weighted into Savillex screw top beakers and then digested using a mixture of double-distilled HF + HNO_3 + HCl. After complete dissolution, 1 ml 8 N HCl + 0.001% H_2O_2 was added to the beaker and then heated to dryness at 80°C. This process was repeated 2 or 3 times to ensure that all cations were converted to chloride species. The final residues were dissolved in 1 ml 8 N HCl + 0.001% H_2O_2 in preparation for ion exchange separation.

The procedure for Cu and Zn purification is modified from *Maréchal et al*. [1999] and outlined in *Liu et al*. [2014a]. Separation of Cu and Zn from matrix elements was accomplished by a single-column ion exchange

chromatography using 2 ml Bio-Rad strong anion resin AG-MP-1M (100–200 mesh, chloride form). Matrix elements (e.g., Na, Mg, Al, K, Ca, Ti, Cr, Ni, Mn, etc.) were eluted in the first 10 ml 8 N HCl + 0.001% H_2O_2, leaving Fe, Co, Cu, and Zn retained on the resin. Cu was collected in the following 26 ml 8 N HCl + 0.001% H_2O_2, and then Co and Fe were eluted as matrix elements using 18 ml 2 N HCl + 0.001% H_2O_2. After further eluting matrix elements and conditioning using 2 ml 0.5 N HNO_3, Zn was collected in the following 10 ml 0.5 N HNO_3. The column chemistry was carried out twice in order to obtain pure Cu and Zn solutions. The Cu and Zn fractions were evaporated to dryness, dissolved in 0.5 ml 3% HNO_3, and then reevaporated to dryness at 80°C, aiming to remove all chlorine. The residues were redissolved in 1 ml 3% HNO_3 in preparation for isotope analysis. The total procedural blanks for Cu and Zn are ~2 ng and ~6 ng, respectively, which are considered negligible relative to ~1.5 μg loaded Cu and Zn. Matrix Na, Ti, Fe, and Mg were checked in the eluted Cu fractions, and Ti, Al, Mg, Cr, and Ni in the eluted Zn fractions, which can significantly impact the accuracy of Cu and Zn isotope analysis due to molecular spectral interference [e.g., *Pribil et al*., 2010; *Liu et al*., 2014a; *Lv et al*., 2016]. The concentration ratios of interference cation (i.e., Na, Ti, Fe, and Mg) to Cu are always <0.09, and cation (i.e., Ti, Al, Mg, Cr, and Ni) to Zn ratios are always <0.23, which are considered negligible and have no significant effect on the accuracy of Cu and Zn isotope analysis [*Liu et al*., 2014a; *Lv et al*., 2016].

3.2. Instrumental Analysis

Copper and Zn isotope ratios were measured using a standard sample-standard bracketing method on a Themo-Finnigan *Neptune plus* MC-ICP-MS at the Isotope Geochemistry Laboratory of the China University of Geosciences, Beijing. Prior to analysis, unknown samples and standards were diluted to 100 ppb for Cu and 200 ppb for Zn in 3% HNO_3, respectively. Both Cu and Zn isotope measurements were performed using wet plasma at low-resolution mode, and each measurement consists of 3 or 4 blocks of 40 cycles with ~8 s integration. Copper and Zn isotopic data are reported in standard δ notation in per mil against international reference materials SRM NIST 976 and JMC 3-0749L, respectively:

$$n\delta^{65}Cu = \left[\left(^{65}Cu/^{63}Cu\right)_{sample}/\left(^{65}Cu/^{63}Cu\right)_{NIST\ 976}\text{-}1\right]\times 1000$$

$$n\delta^{66\ or\ 68}Zn = \left[\left(^{66\ or\ 68}Zn/^{64}Zn\right)_{sample}/\left(^{66\ or\ 68}Zn/^{64}Zn\right)_{JMC\ 3\text{-}0749\ L}\text{-}1\right]\times 1000$$

The long-term external reproducibility is ±0.05‰ (2SD) for both δ^{65}Cu and δ^{66}Zn [*Liu et al*., 2014a, 2016]. δ^{65}Cu and δ^{66}Zn values of international rock standards (e.g., BHVO-2, BCR-2, and BIR-1a) obtained in this study (Table 1) agree well within error with those reported by previous studies [*Archer and Vance*, 2004; *Chen et al*., 2013, 2016; *Bigalke et al*., 2010; *Liu et al*., 2014a, 2014b, 2015; *Sossi et al*., 2015; *Savage et al*., 2015; *Lv et al*., 2016]. In a three-isotope plot (δ^{68}Zn versus δ^{66}Zn; not shown), all measured samples, including international rock standards and AOC samples, define a line with a slope of 0.4998, indicating mass-dependent fractionation. This further indicates insignificant analytical artifacts from unresolved isobaric interferences on Zn isotopes.

4. Results

The Cu and Zn concentrations and isotopic compositions of all the investigated rocks from IODP Site 1256 are listed in Table 1. Rocks from the volcanic section show a relatively small range of Cu (47.5 to 93.7 ppm) and Zn (66.5 to 137 ppm) concentrations and display relatively limited δ^{65}Cu (−0.02 to 0.14‰) and δ^{66}Zn (0.18 to 0.36‰) variations (Figure 3), except for an altered basalt (57R/2, 648.02 m bsf) that has a slightly higher δ^{65}Cu value of 0.23‰ (Figure 3c). Rocks from the transition zone, having Cu from 69.2 to 86.1 ppm and Zn from 99.6 to 132 ppm, have δ^{65}Cu of 0.05 to 0.12‰ and δ^{66}Zn of ca. 0.21‰) (Figure 3). With the exception of a volcanic breccia (140R/1, 1114.72 m bsf) that has very high Cu (16836 ppm) and Zn (237.8 ppm) contents, rocks from the sheeted dyke complex and the plutonic complex have Cu and Zn contents ranging from 13.0 to 198.8 ppm and from 27.1 to193.3 ppm, respectively (Figures 3a and 3b). They have δ^{65}Cu and δ^{66}Zn ranging from −0.50 to 0.90‰ and 0.19 to 0.55‰, respectively (Figures 3c and 3d), exceeding the ranges of mid-ocean ridge basalts (MORBs) (δ^{65}Cu = 0.07 ± 0.06‰ [*Liu et al*., 2015; *Savage et al*., 2015]; δ^{66}Zn = 0.28 ± 0.05‰ [*Ben Othman et al*., 2006; *Chen et al*., 2013]).

Table 1. Copper and Zn Concentrations and Isotopic Compositions of the In Situ Core Samples from IODP Site 1256 in the Eastern Equatorial Pacific

Cor/Sc[a]	T-B (cm)	Depth (m bsf)	Sample Description	Li/Yb[b]	$\delta^{18}O^{b}$ ‰	Cu[b] (ppm)	$\delta^{65}Cu^{c}$ (‰)	2SD[d]	Zn[b] (ppm)	$\delta^{66}Zn^{c}$ (‰)	2SD[d]	$\delta^{68}Zn$ (‰)	2SD[d]	N[e]
			The Volcanic Section											
6R/2	3–11	258.46	coarse-grained altered basalt	1.75		60.9	0.05	0.04	92.9	0.27	0.01	0.54	0.01	3
8R/1	101–108	276.51	fine-grained basalt	1.38	6.2	47.5	0.10	0.02	72.7	0.31	0.04	0.61	0.03	3
12R/8	71–79	351.21	microcrystalline basalt	1.26	6.4	65.4	0.09	0.01	104	0.25	0.02	0.51	0.03	3
27R/1	130–137	446.70	microcrystalline basalt	1.62	7.2	80.8	0.08	0.02	96.5	0.26	0.06	0.52	0.02	3
32R/1	114–120	476.34	microcrystalline basalt	1.47	6.1	64.6	0.07	0.03	87.7	0.32	0.04	0.63	0.03	3
43R2W	48–54	535.88	patchy altered basalt	2.45		93.7	0.02	0.03	75.1	0.27	0.10	0.53	0.18	*3/4*
46R1W	67–69	562.17	altered basalts	4.04	6.4	75.6	0.01	0.08	89.3	0.32	0.07	0.63	0.12	*3/4*
51R1	52–54	596.62	altered basalts	3.46	7.5	91.3	−0.02	0.09	78.5	0.28	0.03	0.54	0.18	*3/4*
55R2W	64–68	629.48	microcrystalline basalt	3.23		76.9	0.01	0.10	81.1	0.26	0.09	0.52	0.16	*3/4*
57R/2	117–127	648.02	red + green altered basalt	5.93	8.6	73.0	0.23	0.05	66.5	0.32	0.04	0.63	0.04	3
Replicate[f]							0.26	0.09						
74R1W	118–122	748.38	patchy basalt	3.62	7.2	72.8	0.05	0.08	94.8	0.25	0.07	0.50	0.15	3
75R/1	131–133	753.05	patchy basalt	1.17	6.8	78.0	0.07	0.01	96.1	0.25	0.01	0.51	0.02	3
80R/1	103–107	781.47	aphyric cryptocrystalline basalt	0.99	6.3	83.8	0.03	0.01	77.8	0.30	0.03	0.59	0.06	3
80R/2	92–102	781.47	fine-grained basalt with mixed halo	1.28		83.8	0.03	0.03	77.8	0.30	0.03	0.59	0.03	3
87R/2	66–68	831.06	phyric fine-grained basalt	1.50	6.8	89.5	0.14	0.06	87.7	0.18	0.06	0.37	0.06	3
89R/1	70–73	840.68	phyric cryptocrystalline basalt	1.32		84.3	0.07	0.04	77.6	0.27	0.03	0.55	0.03	3
96R/1	29–31	893.29	aphyric microcrystalline basalt	0.98	6.0	85.8	0.02	0.05	72.2	0.25	0.03	0.52	0.04	3
99R/2	101–120	909.63	fine-grained background alteration	1.45		81.4	0.07	0.02	88.3	0.29	0.07	0.57	0.03	3
114R/2	54–56	990.04	altered phyric microcrystalline basalt	1.03	6.6	85.2	0.07	0.03	137	0.36	0.02	0.72	0.05	3
			The Lava-Dyke Transition Zone											
117R/1	97–107	1004.17	fine-grained cataclastic basalt	1.00		86.1	0.05	0.07	99.6	0.22	0.02	0.44	0.04	3
128R/1	58–63	1056.77	fine-grained background basalt	0.69	8.1	69.2	0.12	0.03	132.0	0.21	0.03	0.42	0.03	3
			The Sheeted Dyke Complex											
129R/1	34–51	1061.51	fine-grained background basalt	0.69	4.8	69.1	0.01	0.06	90.5	0.25	0.01	0.53	0.12	3
135R/1	54–64	1090.86	patchy microcrystalline basalt	0.81	3.8	75.6	0.11	0.06	166	0.19	0.04	0.39	0.04	3
140R/1	76–79	1114.72	volcanic breccia	3.69	5.5	16836	0.01	0.07	238	0.23	0.01	0.49	0.05	3
147R/1	40–48	1145.98	doleritic basalt	0.96		102	0.07	0.06	108	0.20	0.03	0.40	0.06	3
147R/1	75–77	1145.98	aphyric fine-grained dolerite	0.69	5.1	78.5	0.05	0.03	92.4	0.25	0.04	0.50	0.02	3
163R/3	59–62	1219.91	phyric cryptocrystalline basalt	0.67	4.4	71.7	0.07	0.07	87.4	0.24	0.02	0.48	0.06	3
Cor/Sc[a]	T-B	Depth	Sample	Li/	$\delta^{18}O^{b}$	Cu[b]	$\delta^{65}Cu^{c}$	2SD[d]	Zn[b]	$\delta^{66}Zn^{c}$	2SD[d]	$\delta^{68}Zn^{c}$	2SD[d]	N[e]
	cm	m bsf	description	Yb[b]	‰	ppm	‰		ppm	‰		‰		
165R/3	101–103	1230.19	aphyric microcrystalline basalt	0.38	4.3	64.2	0.07	0.04	112.3	0.27	0.01	0.54	0.09	3
173R/2	6–10	1260.60	phyric medium- to fine-grained basalt	0.78	4.5	84.5	0.10	0.06	105.6	0.22	0.07	0.44	0.07	3
174R/1	130–134	1266.13	aphyric fine-grained basalt	0.35	3.6	89.6	0.08	0.05	193.3	0.20	0.02	0.40	0.04	3
175R/1	58–62	1272.05	aphyric cryptocrystalline basalt	0.40	3.9	73.9	0.15	0.07	99.8	0.30	0.03	0.61	0.03	3
176R/1	133–136	1277.27	aphyric fine-grained basalt	0.35	3.5	13.0	0.10	0.04	191.7	0.25	0.02	0.50	0.05	3
176R/2	22–25	1278.03	ahyric fine-grained basalt	0.26	3.8	58.6	0.09	0.01	140.6	0.27	0.02	0.54	0.03	3
182R/1	25–28	1305.09	aphyric fine-grained basalt	0.42	4.0	198.8	0.15	0.01	70.2	0.32	0.05	0.65	0.09	3
184R/1	98–104	1314.50	aphyric fine-grained basalt	0.38	3.1	77.0	−0.50	0.01	32.0	0.27	0.03	0.54	0.04	3
Replicate[f]							−0.48	0.01						
187R/1	15–17	1325.88	aphyric microcrystalline basalt	0.29	3.2	95.8	0.12	0.06	46.1	0.22	0.04	0.48	0.04	3
196R/1	30–32	1363.86	aphyric fine-grained basalt	0.40	3.4	46.6	0.90	0.02	52.9	0.40	0.02	0.80	0.02	3
Replicate							0.89	0.01						3
202R/1	37–42	1373.05	aphyric fine-gained basalt	0.28	3.0	47.0	0.20	0.01	52.9	0.55	0.03	1.09	0.07	3
Replicate										0.51	0.03	1.05	0.11	3
207R/1	10–15	1390.80	aphyric cryptocrystlalline basalt	0.29	3.3	82.0	0.49	0.04	49.9	0.42	0.01	0.84	0.04	3
Replicate							0.46	0.04						3
209R/1	15–19	1396.65	aphyric microcrystalline basalt	0.32	3.4	29.0	0.51	0.01	51.6	0.50	0.03	1.00	0.04	3

AGU Journal of Geophysical Research: Solid Earth

10.1002/2016JB013095

Journal of Geophysical Research: Solid Earth

10.1002/2016JB013095

Table 1. (continued)

Cor/Sc[a]	T-B (cm)	Depth (m bsf)	Sample Description	Li/Yb[b]	$\delta^{18}O$[b] ‰	Cu[b] (ppm)	$\delta^{65}Cu$[c] (‰)	2SD[d]	Zn[b] (ppm)	$\delta^{66}Zn$[c] (‰)	2SD[d]	$\delta^{68}Zn$ (‰)	2SD[d]	N[e]
Replicate										0.46	0.07	0.93	0.18	3
			The Plutonic Complex											
214R/2	50–55	1413.55	disseminated oxide gabbro	0.63	3.7	64.5	−0.06	0.03	33.6	0.33	0.04	0.68	0.02	3
217R/1	4–9	1421.77	disseminated oxide gabbro	0.88	3.8	121.1	−0.07	0.03	27.1	0.21	0.03	0.45	0.04	3
222R/2	25–35	1446.37	green altered gabbro	0.52		55.2	−0.05	0.02	30.6	0.34	0.07	0.70	0.05	3
223R/2	41–48	1450.68	olivine gabbronorite	0.68	4.0	85.0	−0.43	0.02	37.8	0.38	0.04	0.78	0.07	3
Replicate							−0.44	0.01						
230R/1	68–72	1483.72	fine-grained opx bearing oxide gabbro	0.50	4.6	176.5	0.12	0.00	47.0	0.40	0.03	0.84	0.04	3
230R/2	36–40	1484.99	disseminated oxide gabbro-gabbronorite	0.61	4.8	104.7	0.20	0.04	55.2	0.36	0.03	0.75	0.03	3
231R/3	21–27	1488.80	oxide gabbronorite	0.68	4.9	75.8	−0.16	0.03	51.8	0.38	0.05	0.76	0.05	3
231R/3	80–98	1491.36	opx bearing gabbro	0.88		94.4	−0.09	0.01	51.0	0.25	0.03	0.53	0.02	3
234R/1	19–22	1502.76	fine-grained basalt	0.57	4.4	36.2	−0.01	0.02	95.2	0.29	0.01	0.57	0.06	3
BHVO-2							0.15	0.05		0.35	0.03	0.69	0.06	3
BCR-2							0.19	0.02		0.27	0.02	0.52	0.06	3
BCR-2							0.15	0.05		0.26	0.04	0.52	0.06	3
BCR-2							0.19	0.08		0.31	0.06	0.61	0.08	3
Average							0.17	0.03		0.28	0.05	0.55	0.05	
BIR-1a							0.02	0.04		0.22	0.00	0.49	0.03	3

[a]Except for two samples (6R/2 and 8R/1) that were collected from the Hole 1256C, all the samples were collected from the Hole 1256D.

[b]Li/Yb ratios for rocks above 750 m bsf were calculated from Li and Yb concentrations newly determined by solution ICP-MS at the University of Houston. Cu and Zn concentrations for rocks above 750 m bsf were newly measured by comparison of signal intensities with 100 ppb GSB Cu and 200 ppb GSB Zn, in-house standards [*Liu et al*., 2014a]. O isotopic data for all samples as well as Li/Yb ratios and Cu-Zn concentrations for samples below 750 m bsf were sourced from *Gao et al*. [2012].

[c]$\delta^{65}Cu = (({}^{65}Cu/{}^{63}Cu)_{sample}/({}^{65}Cu/{}^{63}Cu)_{NIST\ 976} - 1) \times 1000$, where NIST 976 is the international Cu isotope standard. $\delta^{66\ or\ 68}Zn = (({}^{66\ or\ 68}Zn/{}^{64}Zn)_{sample}/({}^{66\ or\ 68}Zn/{}^{64}Zn)_{Lyon\text{-}JMC} - 1) \times 1000$, where Lyon-JMC represents the JMC 3-0749L international Zn isotope standard.

[d]The 2SD = 2 two times the standard deviation of the population of *n* repeat measurements of a sample solution.

[e]*N* represents the times of repeat measurements of the same purification solution by MC-ICP-MS. The italic *3/4* denote that Cu isotope measurements were repeated 3 times and Zn isotope measurements 4 times.

[f]Replicate = repeat sample dissolution, purified column chemistry and MC-ICPMS analysis.

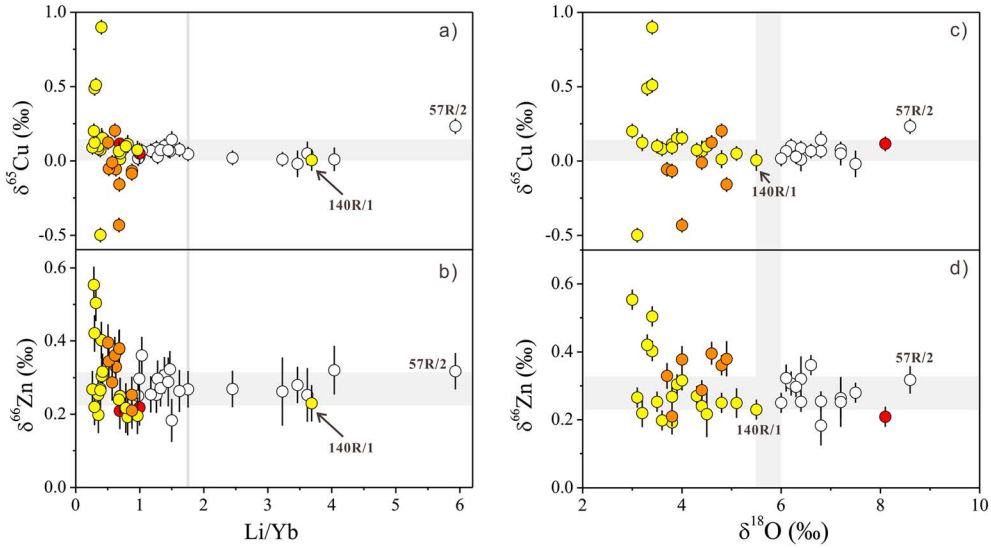

Figure 4. Li/Yb ratio versus (a) δ^{65}Cu and (b) δ^{66}Zn as well as δ^{18}O versus (c) δ^{65}Cu and (d) δ^{66}Zn in the studied AOC samples at IODP Site 1256. The vertical gray bars denote the average Li/Yb ratio (1.75) and δ^{18}O of MORB [*Harmon and Hoefs*, 1995; *Gao et al*., 2012], while the parallel gray bars represent the ranges of δ^{65}Cu and δ^{66}Zn of MORB [*Chen et al*., 2013; *Liu et al*., 2015; *Savage et al*., 2015]. Symbols are the same as those in Figure 2, and the data are taken from Table 1. (For interpretation of the references to color in this figure legend, the reader is referred to the Web version of this article).

5. Discussion

5.1. Distribution of Cu and Zn and Their Isotopes in the Oceanic Crust

5.1.1. The Volcanic Section

Overall, the volcanic section is slightly to moderately altered with a highly altered 0.41 m interval at 648 m bsf that has been interpreted as the presence of a narrow zone of focused fluid flow [*Alt et al*., 2010]. Estimation from oxygen isotopes of secondary minerals (i.e., saponite, celadonite, quartz, and anhydrite) indicates that this section was altered by seawater at temperatures of ~50 to ~135°C (Figure 2a) [*Alt et al*., 2010], consistent with the elevated δ^{18}O relative to MORB observed in this section (Figure 2b). Sample 57R/2 (648.02 m bsf) collected from the zone of focused fluid flow has a heavier Cu isotopic composition relative to MORB (Figure 3c) and the highest δ^{18}O and Li/Yb among the investigated samples (Figures 2b and 2c). Thus, such heavy Cu isotopic composition in sample 57R/2 might be attributed to Cu isotope fractionation with preferential loss of ^{63}Cu to the fluid during fluid-rock interaction at an extreme condition (i.e., focused fluid flow). Lithium/Yb can be used to indicate fluid-rock interaction intensity and δ^{18}O values reflect the variations of alteration temperatures during oceanic crust alteration [e.g., *Muehlenbachs and Clayton*, 1972; *Gao et al*., 2012]. The high δ^{18}O values are in accordance with low alteration temperatures ($<$200°C) in the volcanic section (Figures 2a and 2b). Under such low temperatures, high ($>$1.75) and low ($<$1.75) Li/Yb ratios denote high and low seawater/rock ratios, respectively [*Gao et al*., 2012]. Except for sample 57R/2, the rest of the rocks in the volcanic section have MORB-like Cu and Zn isotopic compositions (Figures 3c and 3d). In addition, there exist no correlations of δ^{65}Cu (δ^{66}Zn) with Li/Yb (Figure 4) and δ^{18}O (Figure 4). These features suggest that alteration of oceanic crust at low temperatures results in limited Cu and Zn isotope fractionation at bulk rock scale, regardless of seawater/rock ratios.

Copper and Zn have a very low solubility in fluids at temperatures of $<$350°C and thus can be regarded as nearly conservative elements during low-*T* alteration of oceanic crust [*Seewald and Seyfried*, 1990]. This is supported by the observation that most of the rocks in the volcanic section show no significant losses of Cu and Zn relative to MORB (Figures 3a and 3b). The conservative behavior at low temperatures may be responsible for the relatively limited ranges of δ^{65}Cu and δ^{66}Zn values in the volcanic section rocks. Exceptionally, some altered rocks show loss of Cu during fluid-rock interactions, as indicated by their low Cu contents (e.g., 47.5 ppm, 8R/1 at 276.5 m bsf) (Figure 3a). However, their Cu isotopic compositions are similar to those of MORB (Figure 3c). This can be ascribed to there being no redox changes during the Cu leaching processes, because limited Cu isotope fractionation occurs during precipitation and dissolution of Cu-rich minerals

(e.g., sulfide) without redox changes [e.g., *Ehrlich et al*., 2004]. Alternatively, the lack of Cu isotope fractionation in this sample may be due to reservoir effects. Rocks with very high Cu contents (>150 ppm), reflecting sulfide accumulation, have MORB-like Cu isotopic compositions (Figures 3a and 3c), potentially suggesting that coexisting primary minerals (e.g., sulfide and silicate) and basaltic glass have similar Cu isotopic compositions. Certain tiny Cu-bearing minerals might have been dissolved completely during fluid-rock interactions, leading to Cu depletion but no Cu isotope variations in the residual rocks.

Magnesite-ilmenite thermo-oxybarometery results show relatively high temperatures (760–850°C) and low oxygen fugacities (ΔNNO = −2.2 to −1.1) in the lava pond samples from the Site 1256 volcanic section (Figure 2d) [*Koepke et al*., 2008; *Dziony et al*., 2014]. Such *T*-*f*(O_2) conditions were established at the end of the magmatic stage or during the onset of rapid cooling of this unit [*Dziony et al*., 2014]. This suggests that these lava pond samples record the oxidation state of the magma. That is, low-*T* alteration did not increase their oxygen fugacity. Given no systematic change with depth in oxidation state of rocks in this section [*Wilson et al*., 2006], other samples should have oxygen fugacity similar to those of the two lava pond rocks. Under conditions of such low oxygen fugacity, Cu is always present as Cu^{+1} in magmas and altered rocks during oceanic crust accretion and alteration [e.g., *Ripley et al*., 2002; *Dekov et al*., 2013].

Collectively, low solubility of Cu and Zn in hydrothermal fluids at low alteration temperatures and the absence of redox changes at low oxygen fugacity are the major factors resulting in the limited Cu and Zn isotope fractionation in the Site 1256 volcanic section.

5.1.2. The Transition Zone

Subsurface mixing of upwelling hydrothermal fluids with cooler seawater in the transition zone is illustrated by the stepwise increase in alteration grade and temperatures (Figure 2a). Elevated whole-rock $^{87}Sr/^{86}Sr$ ratios relative to MORB also signify the influence of seawater [*Harris et al*., 2015]. However, seawater has inconsequential concentrations of Cu and Zn compared to hydrothermal fluids [*Seewald and Seyfried*, 1990; *John et al*., 2008; *Little et al*., 2014b]. When the upwelling high-*T* fluids mixed with cool seawater, the Cu and Zn budgets of the mixed fluids are mainly controlled by Cu and Zn leached from basalts in the high-*T* deep zones. In other words, the mixed fluids should have Cu and Zn isotopic compositions similar to high-*T* hydrothermal fluids rather than seawater that has $\delta^{65}Cu$ of ~0.90‰ and $\delta^{66}Zn$ of ~0.50‰ [*Vance et al*., 2008; *Little et al*., 2014b].

Measurements of active vent fluids have revealed that high-*T* hydrothermal fluids (>300°C) have $\delta^{66}Zn$ values similar to those of MORB [*John et al*., 2008]. Thus, the mixed fluids should have a MORB-like Zn isotopic composition. In addition, temperatures of the mixed fluids should be similar to those recorded in rocks from the transition zone (~130–180°C, Figure 2a). Thus, interaction of such low-*T* fluids is unlikely to alter the Zn isotopic compositions of the transition zone rocks and thus explain the limited range of $\delta^{66}Zn$ values observed (~0.21‰) (Figure 3d). No direct measurements of hydrothermal fluids for Cu isotopic compositions have been carried out so far. Copper-rich sulfide in hydrothermal systems show extremely large $\delta^{65}Cu$ variations from −17.0 to 10.0‰ [e.g., *Rouxel et al*., 2004; *Mason et al*., 2005; *Wilkinson et al*., 2005; *Mathur et al*., 2005, 2009, 2012; *Markl et al*., 2006; *Kim et al*., 2014]. However, such Cu isotopic variations cannot directly reflect those of hydrothermal fluids, because of Cu isotope fractionation induced by kinetic processes (e.g., diffusion), redox reactions, and/or multiple cycles of sulfide precipitation and dissolution. Previous experimental results showed that redox reactions from Cu^{2+} to Cu^{+} can cause Cu isotope fractionation of ~4‰ at 20°C [*Zhu et al*., 2002; *Ehrlich et al*., 2004], much smaller than the $\delta^{65}Cu$ range of hydrothermal sulfides described above. Although the magnitude and direction of diffusion-driven kinetic Cu isotope fractionation during sulfide precipitation are unclear, the ~27‰ variations in $\delta^{65}Cu$ of sulfides, to some extent, must reflect the heterogeneous Cu isotopic compositions of hydrothermal fluids that precipitated sulfides. Thus, we infer that the mixed fluids may have a MORB-like Cu isotopic composition or a distinct Cu isotopic composition from MORB. The similarity of $\delta^{65}Cu$ between the transition zone rocks and MORB (Figure 3c) implies that limited Cu isotope variation occurred during oceanic crust alteration by the low-*T* mixed fluids.

5.1.3. The Sheeted Dyke Complex and Plutonic Complex

Copper and Zn concentrations are much more variable in the sheeted dyke complex and the plutonic complex (Figures 3a and 3b), consistent with the observation of *Alt et al*. [2010]. The high Zn concentrations (>150 ppm) (Figure 3b) and the extremely high Cu concentration in the volcanic breccia

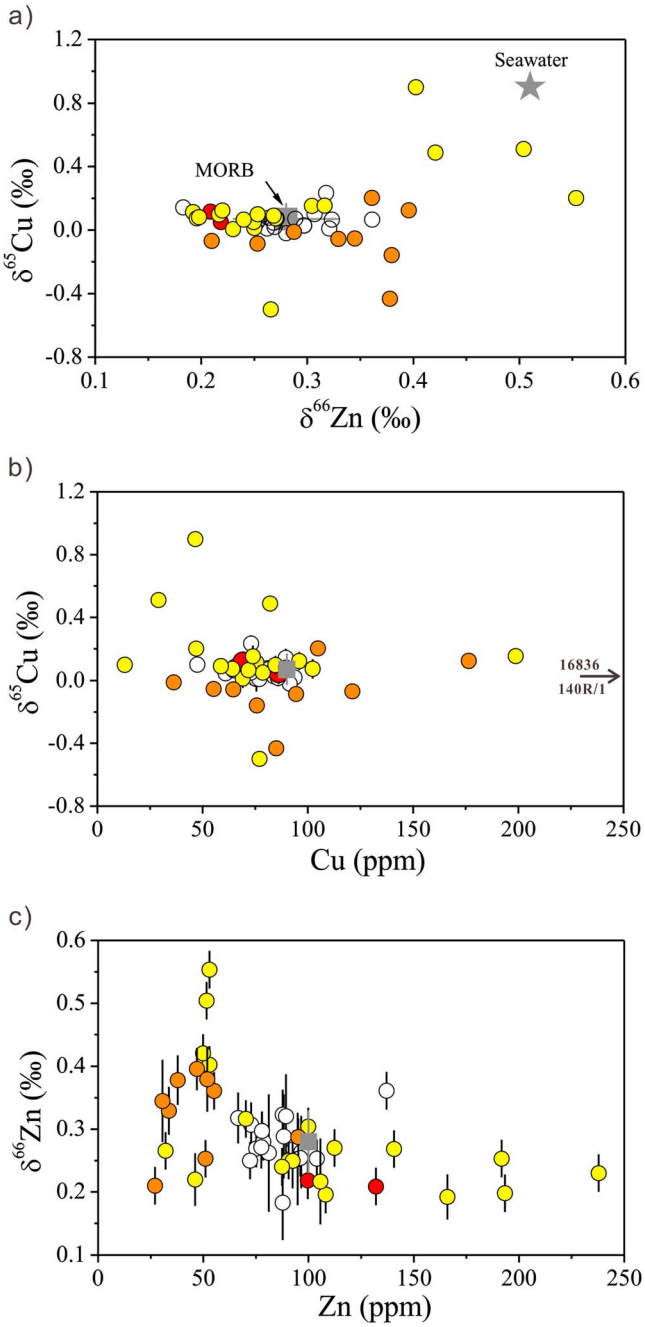

Figure 5. (a) δ^{66}Zn versus δ^{65}Cu, (b) Cu versus δ^{65}Cu, and (c) Zn versus δ^{66}Zn in the studied AOC samples at IODP Site 1256. The average Cu and Zn concentrations for MORB (gray square) are 90 ppm and 100 ppm, respectively [*Le Roux et al.*, 2010; *Fellows and Canil*, 2012]. Average MORB and seawater δ^{65}Cu and δ^{66}Zn values are taken from references *Vance et al.* [2008], *Chen et al.* [2013], *Little et al.* [2014b], *Liu et al.* [2015], and *Savage et al.* [2015]. Symbols are the same as those in Figure 2, and the data are taken from Table 1. (For interpretation of the references to color in this figure legend, the reader is referred to the Web version of this article).

(140R/1, 1114.72 m bsf) (Figure 3a) reflect local sphalerite/chalcopyrite mineralization, consistent with the occurrence of sphalerite-/chalcopyrite-bearing veins and mineralized breccia in the sheeted dykes [*Alt et al.*, 2010]. *Alt et al.* [2010] found that Cu-rich (>150 ppm) altered gabbros contain recrystallized igneous sulfides, reflecting igneous accumulation of Cu-Fe and Fe sulfides. The high Cu concentration (>150 ppm) in a gabbro (Figure 3a) thus can be reasonably explained by igneous Cu-rich sulfide accumulation. Variable depletions in Cu below ~1180 m bsf and in Zn below ~1300 m bsf can be observed (Figures 3a and 3b)]*Alt et al.*, 2010]. Copper in seafloor basaltic rocks is dominantly hosted by primary chalcopyrite with trace amounts of Cu hosted by primary magmatic Fe sulfides and silicates (e.g., olivine, basaltic glass) [*Dekov et al.*, 2013]. Zn in seafloor basalts is hosted by primary magmatic sulfides (e.g., sphalerite) and silicates (e.g., olivine, pyroxene). Due to high solubility of Cu and Zn in hydrothermal fluids at temperatures of >350°C [*Seewald and Seyfried*, 1990], such metal depletions probably resulted from high-*T* hydrothermal alteration of primary minerals (e.g., sulfide and olivine) and basaltic glass, which might be considered as a principal process causing release of Cu and Zn from seafloor basaltic rocks.

Relative to MORB, larger δ^{65}Cu and δ^{66}Zn variations are observed in the lowermost sheeted dyke and the plutonic complex (Figures 3c and 3d). The localized variations in δ^{65}Cu and δ^{66}Zn reflect a channelized fluid flow, as revealed by increases in ^{87}Sr/^{86}Sr in the same location of Hole 1256D [*Harris et al.*, 2015]. The relationship between δ^{65}Cu and δ^{66}Zn cannot be simply explained by a binary mixing between MORB and seawater (Figure 5a). It is noted that samples with large δ^{65}Cu and δ^{66}Zn variations are generally accompanied by lower Li/Yb ratios (Figures 4a and 4b), lower δ^{18}O values (Figures 4c and 4d), and lower Cu and

Table 2. Mass Balance Model for Cu and Zn in the Intact Oceanic Crust at IODP Site 1256

		Depth Interval[b]	Avg. Cu[c]	Avg. δ^{65}Cu[c]		Avg. Zn[c]	Avg. δ^{66}Zn[c]	2SD
Lithostratigraphy	N[a]	(m)	(ppm)	(‰)	2SD	(ppm)	(‰)	
Volcanic section	19	754.5	78	0.07	0.11	84	0.28	0.08
Transition zone	2	56.7	78	0.08	0.09	116	0.21	0.01
Upper sheeted dyke	15 (14)	287.4	1199 (82)	0.05 (0.05)	0.31	118 (110)	0.24 (0.25)	0.07
Lowermost sheeted dyke	4	58.3	51	0.53	0.57	52	0.47	0.14
Plutonic complex	9	114.7	81	−0.15	0.37	32	0.32	0.15
Bulk AOC[d]				0.05 (0.07)	0.03		0.27 (0.26)	0.01

[a] N denotes the number of samples analyzed and used for the calculation of average values in each section. The numbers in parentheses denote the values calculated without consideration of the volcanic breccia (140R/1, 1114.72 m bsf) which has an abnormally high Cu content (Table 1).
[b] The depth interval for each section is cited from *Teagle et al.* [2006, 2012]. As bulk rocks from different sections have similar density [*Teagle et al.*, 2006], the total mass of each section is proportional to its depth interval that was used to calculate the concentration-weighted average δ^{65}Cu and δ^{66}Zn values of bulk oceanic crust at IODP Site 1256.
[c] Average (Avg.) Cu and Zn contents as well as δ^{65}Cu and δ^{66}Zn values for each section analyzed here.
[d] Weighted average δ^{65}Cu and δ^{66}Zn values of the bulk altered oceanic crust (AOC) derived from mass balance calculation, using Cu and Zn percentage in the bulk oceanic crust of each section as the weight.

Zn contents (Figures 5b and 5c) relative to MORB. These features suggest that intense hydrothermal fluid-rock interactions at high temperatures, generally associated with Cu and Zn depletions of rocks, result in the observed Cu and Zn isotope variations.

Experimental and theoretical works have demonstrated that redox changes from Cu^{+1} to Cu^{+2} can result in significant Cu isotope fractionation, with the latter being enriched in the heavy isotope (^{65}Cu) [e.g., *Zhu et al.*, 2002; *Ehrlich et al.*, 2004; *Mathur et al.*, 2005; *Fujii et al.*, 2013]. At the range of fO_2 typical of basaltic rocks, Cu^{1+} is the dominant valence state and dominantly hosted by sulfide [e.g., *Ripley et al.*, 2002; *Lee et al.*, 2012]. High fO_2 in the lowermost dykes and the plutonic complex (Figure 2d) is favorable for oxidizing Cu^{+1} in altered rocks to Cu^{+2} in hydrothermal fluids, leaving the residual Cu enriched in light isotopes. This may explain low δ^{65}Cu values (down to −0.50‰) in some rocks (Figure 3c). This explanation is consistent with the results of previous leach experiments that the residue is enriched in ^{63}Cu relative to starting Cu-sulfides (e.g., chalcopyrite, bornite, and chalcocite) [*Fernandez and Borrok*, 2009; *Kimball et al.*, 2009; *Wall et al.*, 2011]. In addition to redox changes, Cu isotope fractionation can occur between different Cu species in hydrothermal fluids [*Seo et al.*, 2007; *Fujii et al.*, 2013]. Among Cu^{1-} species, $[CuCl_3]^{1-}$ is the most depleted in ^{65}Cu with $\Delta^{65}Cu_{[Cu(HS)2]1- - [CuCl3]1-}$ of 0.15 even at temperature of 600°C [*Seo et al.*, 2007], while among Cu^{2-} species, $CuCl_2$ is the most depleted [*Fujii et al.*, 2013]. Thus, $[CuCl_3]^{1-}$ in hydrothermal fluids should be enriched in ^{63}Cu relative to Cu sulfide in seafloor basaltic rocks. Previous studies show that high-T hydrothermal fluids contain large amounts of Cl^- (at least 300 to 700 mM) [e.g., *Von Damm et al.*, 1985; *John et al.*, 2008]. Thus, Cu isotope fractionation between sulfide and $[CuCl_3]^{1-}$ with increasing hydrothermal extraction of Cu in the high-T reaction zone may explain high δ^{65}Cu values observed in rocks from the lowermost dyke (Figures 3c and 5b).

Theoretical calculations [*Black et al.*, 2011] and studies of ore minerals [*Wilkinson et al.*, 2005] and hydrothermal vent fluids [*John et al.*, 2008] suggest that Zn sulfide and chloride complexes are enriched in light isotopes (^{64}Zn). Thus, Zn isotope fractionation between basaltic rocks and Zn sulfide and chloride complexes in hydrothermal fluids during the process of Zn loss would interpret the heavier Zn isotopic compositions and lower Zn concentrations relative to MORB, observed in most rocks from the lowermost dyke and the plutonic complex (Figures 3b, 3d, and 5c).

5.2. Implications

In this study, the bulk AOC at IODP Site 1256 has concentration-weighted average δ^{65}Cu of 0.05 ± 0.03‰ and δ^{66}Zn of 0.27 ± 0.01‰ (Table 2), similar to those of the mantle or fresh MORB (δ^{65}Cu = 0.06 ± 0.20‰ [*Liu et al.*, 2015] or 0.07 ± 0.10‰ [*Savage et al.*, 2015], δ^{66}Zn = 0.28 ± 0.05‰ [*Chen et al.*, 2013]). The findings of mantle-like Cu and Zn isotopic compositions of AOC have important geochemical implications.

Previous studies have shown that orogenic and xenolith peridotites display highly variable δ^{65}Cu from −0.68 to 1.82‰ [*Savage et al.*, 2014; *Liu et al.*, 2015]. It is noted that peridotites characterized by LREE enrichments

and the presence of secondary minerals (e.g., phlogopite) show more heterogeneous Cu isotopic compositions relative to peridotites devoid of metasomatism. *Liu et al*. [2015] also observed that basalts from Eastern China and Kamchatka arc have variable δ^{65}Cu from −0.19 to 0.47‰. Notably, arc lavas with higher Ba/Nb ratios tend to have larger variations in δ^{65}Cu [see *Liu et al*., 2015, Figure 7]. All these features suggest that abnormal δ^{65}Cu observed in peridotites and basalts probably resulted from metasomatism by fluids sourced from hydrothermally altered oceanic crust [*Savage et al*., 2014; *Liu et al*., 2015]. To generate 2.5‰ Cu isotopic variations of the metasomatized peridotites from the mantle-like Cu isotopic composition of the AOC, there must be one or more processes fractionating Cu isotopes significantly. It is well known that slab-derived fluids have high oxygen fugacity above the sulfide-sulfur oxide buffer [*Sun et al*., 2007]. Addition of such oxidizing fluids to mantle peridotites would cause oxidative breakdown of sulfides [e.g., *Liu et al*., 2011]. As ^{65}Cu is preferentially leached into the fluids during sulfide redox reaction [e.g., *Mathur et al*., 2005, 2012], this process results in ^{65}Cu depletion in the metasomatized peridotites and ^{65}Cu enrichment in the fluids. Precipitation of secondary minerals (e.g., Cu-rich sulfides and oxides) from such ^{65}Cu-rich fluids may shift the peridotites to heavy Cu isotopic compositions. Thus, primary sulfide dissolution and secondary mineral precipitation together may explain the highly heterogeneous Cu isotopic compositions observed in metasomatized peridotites.

Liu et al. [2016] recently found that the Eastern China basalts with age of <110 Ma have heavier δ^{66}Zn values (0.30‰ to 0.63‰) relative to the mantle (0.28 ± 0.05‰) [*Chen et al*., 2013]. It is well known that marine carbonates have heavy δ^{66}Zn of 0.91 ± 0.41‰ (2SD, $N = 52$) [*Pichat et al*., 2003]. Together with the fact that these basalts have light Mg isotopic compositions [*Yang et al*., 2012; *Huang et al*., 2015b], *Liu et al*. [2016] attributed such heavy δ^{66}Zn of basalts to the incorporation of marine carbonates into their mantle sources. However, trace element and Sr-Nd-Pb isotopic evidence suggests that the mantle sources of the <110 Ma basalts contain variable amounts of recycled AOC [e.g., *Xu*, 2014]. The mantle-like Zn isotopic composition of the AOC at Site 1256 confirms that the abnormal heavy δ^{66}Zn of the <110 Ma Eastern China basalts should result from recycled marine carbonates rather than recycled AOC. Thus, Zn isotopes can be used as a new and useful tool of tracing deep marine carbonate cycling in the Earth's mantle [*Liu et al*., 2016].

6. Conclusion

This study presents the first combined study of Cu and Zn isotopic compositions on rocks recovered from the intact oceanic crust at IODP Site 1256 in the eastern equatorial Pacific. The following conclusions can be made:

1. Except for one sample at 648.02 m bsf that has slightly heavier Cu isotopic composition compared with MORB, rocks from the volcanic section have MORB-like Cu and Zn isotopic compositions. The limited isotope fractionation is interpreted as the result of limited mobility of Cu and Zn as well as low oxygen fugacity during low-*T* (<200°C) seawater alteration of oceanic crust.
2. Rocks from the transition zone have both δ^{65}Cu and δ^{66}Zn similar to those of MORB. Such features may be ascribed to insignificant Cu and Zn loss and/or gain during alteration of the transition zone rocks by the low-*T* mixed fluids between seawater and high-*T* hydrothermal fluids.
3. The sheeted dyke complex and the plutonic complex exhibit highly variable concentrations of Cu and Zn. The high metal contents reflect local Cu/Zn-rich sulfide accumulation during igneous processes or mineralization, whereas the low contents indicate leaching of metals during hydrothermal alteration at high temperatures (>350°C). Rocks in both sections have variable Cu and Zn isotopic compositions, significantly exceeding the range of MORB. The δ^{65}Cu and δ^{66}Zn variations are coupled with Cu and Zn depletions as well as very low Li/Yb (<1.0) and δ^{18}O (<5‰), indicating that Cu and Zn isotopes can be fractionated during high-temperature hydrothermal alteration of oceanic crust. Redox transformation of Cu as well as Cu and Zn isotope fractionation between altered basaltic rocks and dissolved Cu and Zn species in hydrothermal fluids (e.g., $[CuCl_3]^{1-}$, $Zn(HS)_4^{2-}$) account for such large Cu and Zn variations.
4. The mantle-like average Cu and Zn isotopic compositions of the AOC have at least two important implications. The highly heterogeneous Cu isotopic compositions of the lithospheric mantle may largely result from oxidative sulfide dissolution and secondary mineral precipitation. Zinc isotopes are sensitive to carbonate cycling and can be used as a powerful tool of tracing deep carbon cycling in the Earth's mantle.

Acknowledgments
This work is financially supported by grants from the MOST of China (2016YFC0600404), the National Natural Science Foundation of China (41573018, 41303015, and 41473017), and the Fundamental Research Funds (2-9-2015-299). Help from D.D. Li, Y.W. Lv, and Z.Z. Wang during the course of Cu and Zn isotope analyses is thanked. We also gratefully acknowledge Ryan Mathur and three anonymous reviewers for thorough and constructive comments and suggestions, which greatly improve this manuscript. We also thank Michael Walter for the editorial handling. The data for this paper are listed in Tables 1 and 2 and available by contacting the corresponding author at jianhuang@ustc.edu.cn.

References

Alt, J. C., C. Laverne, R. M. Coggon, D. A. H. Teagle, N. R. Banerjee, S. Morgan, C. E. Smith-Duque, M. Harris, and L. Galli (2010), Subsurface structure of a submarine hydrothermal system in ocean crust formed at the East Pacific Rise, ODP/IODP Site 1256, *Geochem. Geoph. Geosyst.*, *11*, Q10010, doi:10.1029/2010GC003144.

Archer, C., and D. Vance (2004), Mass discrimination correction in multiple-collector plasma source mass spectrometry: An example using Cu and Zn isotopes, *J. Anal. At. Spectrom.*, *19*, 656–665.

Balistrieri, L. S., D. M. Borrok, R. B. Wanty, and W. I. Ridley (2008), Fractionation of Cu and Zn isotopes during adsorption onto amorphous Fe (III) oxyhydroxide: Experimental mixing of acid rock drainage and ambient river water, *Geochim. Cosmochim. Acta*, *72*, 311–328.

Ben Othman, D., J. M. Luck, J. L. Bodinier, N. T. Arndt, and F. Albarède (2006), Cu-Zn isotopic variations in the Earth's mantle, *Geochim. Cosmochim. Acta*, *70*, A46.

Bigalke, M., S. Weyer, and W. Wilcke (2010), Copper isotope fractionation during complexation with insolubilized humic acid, *Environ. Sci. Technol.*, *44*, 5496–5502.

Black, J. R., A. Kavner, and E. A. Schauble (2011), Calculation of equilibrium stable isotope partition function ratios for aqueous zinc complexes and metallic zinc, *Geochim. Cosmochim. Acta*, *75*, 769–783.

Campbell, A. C., T. S. Bowers, C. I. Measures, K. K. Falkner, M. Khadem, and J. M. Edmond (1988a), A time series of vent fluid compositions from 21°N, East Pacific Rise (1979, 1981, 1985), and the Guaymas Basin, Gulf of California (1982, 1985), *J. Geophys. Res.*, *93*, 4537–4549.

Campbell, A. C., et al. (1988b), Chemistry of hot springs on the Mid-Atlantic Ridge, *Nature*, *335*, 514–519.

Chan, L.-H., J. C. Alt, and D. A. H. Teagle (2002), Lithium and lithium isotope profiles through the upper oceanic crust: A study of seawater-basalt exchange at ODP Sites 504B and 896A, *Earth Planet. Sci. Lett.*, *201*, 187–201.

Chen, H., P. S. Savage, F.-Z. Teng, R. T. Helz, and F. Moynier (2013), Zinc isotope fractionation during magmatic differentiation and the isotopic composition of the bulk Earth, *Earth Planet. Sci. Lett.*, *369–370*, 34–42.

Chen, S., Y. Liu, J. Hu, Z. Zhang, Z. Hou, F. Huang, and H. Yu (2016), Zinc isotopic compositions of NIST SRM 683 and whole-rock reference materials, *Geostand. Geoanal. Res.*, *40*, 417–432, doi:10.1111/j.1751-908X.2015.00377.x.

Dekov, V. M., O. Rouxel, D. Asael, U. Hålenius, and F. Munnik (2013), Native Cu from the oceanic crust: Isotopic insights into native metal origin, *Chem. Geol.*, *359*, 136–149.

Doe, B. R. (1994), Zinc, copper, and lead in mid-ocean ridge basalts and the source rock control on Zn/Pb in ocean-ridge hydrothermal deposits, *Geochim. Cosmochim. Acta*, *58*, 2215–2223.

Dziony, W., I. Horn, D. Lattard, J. Koepke, G. Steinhoefel, J. A. Schuessler, and F. Holtz (2014), In-situ Fe isotope ratio determination in Fe–Ti oxides and sulfides from drilled gabbros and basalt from the IODP Hole 1256D in the eastern equatorial Pacific, *Chem. Geol.*, *363*, 101–113.

Ehrlich, S., I. Butler, L. Halicz, D. Rickard, A. Oldroyd, and A. Matthews (2004), Experimental study of the copper isotope fractionation between aqueous Cu(II) and covellite, CuS, *Chem. Geol.*, *209*, 259–269.

Fellows, S. A., and D. Canil (2012), Experimental study of the partitioning of Cu during partial melting of Earth's mantle, *Earth Planet. Sci. Lett.*, *337–338*, 133–143.

Fernandez, A., and D. M. Borrok (2009), Fractionation of Cu, Fe, and Zn isotopes during the oxidative weathering of sulfide-rich rocks, *Chem. Geol.*, *264*, 1–12.

Fujii, T., F. Moynier, M. Abe, K. Nemoto, and F. Albarede (2013), Copper isotope fractionation between aqueous compounds relevant to low temperature geochemistry and biology, *Geochim. Cosmochim. Acta*, *110*, 29–44.

Furnes, H., K. Muehlenbachs, T. Torsvik, I. H. Thorseth, and O. Tumyr (2001), Microbial fractionation of carbon isotopes in altered basaltic glass from the Atlantic Ocean, Lau Basin and Costa Rica Rift, *Chem. Geol.*, *173*, 313–330.

Gao, Y. J., et al. (2012), Downhole variation of lithium and oxygen isotopic compositions of oceanic crust at East Pacific Rise, ODP Site 1256, *Geochem. Geoph. Geosyst.*, *13*, Q1001, doi:10.1029/2012GC004207.

Harmon, R., and J. Hoefs (1995), Oxygen isotope heterogeneity of the mantle deduced from global 18O systematics of basalts from different geotectonic settings, *Contrib. Mineral. Petrol.*, *120*, 95–114.

Harris, M., R. M. Coggon, C. E. Smith-Duque, M. J. Cooper, J. A. Milton, and D. A. H. Teagle (2015), Channelling of hydrothermal fluids during the accretion and evolution of the upper oceanic crust: Sr isotope evidence from ODP Hole 1256D, *Earth Planet. Sci. Lett.*, *416*, 56–66.

Hart, S. R., J. Blusztajn, H. J. B. Dick, P. S. Meyer, and K. Muehlenbachs (1999), The fingerprint of seawater circulation in a 500-meter section of ocean crust gabbros, *Geochim. Cosmochim. Acta*, *63*, 4059–4080.

Huang, J., S. Ke, Y. Gao, Y. Xiao, and S. Li (2015a), Magnesium isotopic compositions of altered oceanic basalts and gabbros from IODP Site 1256 at the East Pacific Rise, *Lithos*, *231*, 53–61.

Huang, J., S.-G. Li, Y. Xiao, S. Ke, W.-Y. Li, and Y. Tian (2015b), Origin of low δ^{26}Mg Cenozoic basalts from South China Block and their geodynamic implications, *Geochim. Cosmochim. Acta*, *164*, 298–317.

John, S. G., O. J. Rouxel, P. R. Craddock, A. M. Engwall, and E. A. Boyle (2008), Zinc stable isotopes in seafloor hydrothermal vent fluids and chimneys, *Earth. Planet. Sci. Lett.*, *269*, 17–28.

Kim, J., J.-W. Moon, I. Lee, Y. Kim, and P. Larson (2014), Copper isotope composition of seafloor hydrothermal vents in back-arc and arc settings, western Pacific, Goldschmidt2014 Conference Abstracts 1249.

Kimball, B. E., R. Mathur, A. C. Dohnalkova, A. J. Wall, R. L. Runkel, and S. L. Brantley (2009), Copper isotope fractionation in acid mine drainage, *Geochim. Cosmochim. Acta*, *73*, 1247–1263.

Koepke, J., D. M. Christie, W. Dziony, F. Holtz, D. Lattard, J. Maclennan, S. Park, B. Scheibner, T. Yamasaki, and S. Yamazaki (2008), Petrography of the dike-gabbro transition at IODP Site 1256 (equatorial Pacific): The evolution of the granoblastic dikes, *Geochem. Geoph. Geosyst.*, *9*, Q07O09, doi:10.1029/2008GC001939.

Lee, C.-T. A., P. Luffi, E. J. Chin, R. Bouchet, R. Dasgupta, D. M. Morton, V. Le Roux, Q.-z. Yin, and D. Jin (2012), Copper systematics in arc magmas and implications for crust-mantle differentiation, *Science*, *336*, 64–68.

Le Roux, V., C. T. A. Lee, and S. J. Turner (2010), Zn/Fe systematics in mafic and ultramafic systems: Implications for detecting major element heterogeneities in the Earth's mantle, *Geochim. Cosmochim. Acta*, *74*, 2779–2796.

Li, D. D., S.-A. Liu, and S. Li (2015), Copper isotope fractionation during adsorption onto kaolinite: Experimental approach and applications, *Chem. Geol.*, *396*, 74–82.

Li, W. Q., S. E. Jackson, N. J. Pearson, and S. Graham (2010), Copper isotopic zonation in the Northparkes porphyry Cu–Au deposit, SE Australia, *Geochim. Cosmochim. Acta*, *74*, 4078–4096.

Little, S. H., D. M. Sherman, D. Vance, and J. R. Hein (2014a), Molecular controls on Cu and Zn isotopic fractionation in Fe–Mn crusts, *Earth Planet. Sci. Lett.*, *396*, 213–222.

Little, S. H., D. Vance, C. Walker-Brown, and W. M. Landing (2014b), The oceanic mass balance of copper and zinc isotopes, investigated by analysis of their inputs, and outputs to ferromanganese oxide sediments, *Geochim. Cosmochim. Acta*, *125*, 673–693.
Liu, J. G., R. L. Rudnick, R. J. Walker, S. Gao, F.-y. Wu, P. M. Piccoli, H. Yuan, W.-l. Xu, and Y.-G. Xu (2011), Mapping lithospheric boundaries using Os isotopes of mantle xenoliths: An example from the North China Craton, *Geochem. Cosmochim. Acta*, *75*, 3881–3902.
Liu, S.-A., D. Li, S. Li, F.-Z. Teng, S. Ke, Y. He, and Y. Lu (2014a), High-precision copper and iron isotope analysis of igneous rock standards by MC-ICP-MS, *J. Anal. At. Spectrom.*, *29*, 122–133.
Liu, S.-A., F.-Z. Teng, S. Li, G.-J. Wei, J.-L. Ma, and D. Li (2014b), Copper and iron isotope fractionation during weathering and pedogenesis: Insights from saprolite profiles, *Geochim. Cosmochim. Acta*, *146*, 59–75.
Liu, S.-A., J. Huang, J. Liu, G. Wörner, W. Yang, Y.-J. Tang, Y. Chen, L.-M. Tang, J.-P. Zheng, and S.-G. Li (2015), Copper isotopic composition of the silicate Earth, *Earth Planet. Sci. Lett.*, *427*, 95–103.
Liu, S.-A., Z.-Z. Wang, S.-G. Li, J. Huang, and W. Yang (2016), Zinc isotope evidence for a large-scale carbonated mantle beneath eastern China, *Earth Planet. Sci. Lett.*, *444*, 169–178.
Lodders, K. (2003), Solar system abundances and condensation temperatures of the elements, *The Astroph. J.*, *591*, 1220–1247.
Lv, Y., S.-A. Liu, J.-M. Zhu, and S. Li (2016), Copper and zinc isotope fractionation during deposition and weathering of highly metalliferous black shales in central China, *Chem. Geol.*, *422*, 82–93.
Maréchal, C. N., P. Télouk, and F. Albarède (1999), Precise analysis of copper and zinc isotopic compositions by plasma-source mass spectrometry, *Chem. Geol.*, *156*, 251–273.
Maréchal, C. N., E. Nicolas, C. Douchat, and F. Albarède (2000), Abundance of zinc isotopes as a marine biogeochemical tracer, *Geochem. Geoph. Geosyst.*, *1*, Q1015, doi:10.1029/1999GC000029.
Markl, G., Y. Lahaye, and G. Schwinn (2006), Copper isotopes as monitors of redox processes in hydrothermal mineralization, *Geochim. Cosmochim. Acta*, *70*, 4215–4228.
Mason, T. F. D., D. J. Weiss, J. B. Chapman, J. J. Wilkinson, S. G. Tessalina, B. Spiro, M. S. A. Horstwood, J. Spratt, and B. J. Coles (2005), Zn and Cu isotopic variability in the Alexandrinka volcanic-hosted massive sulphide (VHMS) ore deposit, Urals, Russia, *Chem. Geol.*, *221*, 170–187.
Mathur, R., and M. S. Fantle (2015), Copper isotopic perspectives on supergene processes: implications for the global Cu cycle, *Elements*, *11*, 323–329.
Mathur, R., J. Ruiz, S. Titley, L. Liermann, H. Buss, and S. Brantley (2005), Cu isotopic fractionation in the supergene environment with and without bacteria, *Geochim. Cosmochim. Acta*, *69*, 5233–5246.
Mathur, R., S. Titley, F. Barra, S. Brantley, M. Wilson, A. Phillips, F. Munizaga, V. Maksaev, J. Vervoort, and G. Hart (2009), Exploration potential of Cu isotope fractionation in porphyry copper deposits, *J. Geochem. Explor.*, *102*, 1–6.
Mathur, R., J. Ruiz, M. J. Casselman, P. Megaw, and R. van Egmond (2012), Use of Cu isotopes to distinguish primary and secondary Cu mineralization in the Caariaco Norte porphyry copper deposit, Northern Peru, *Mineral. Deposita*, *47*, 755–762.
Muehlenbachs, K., and R. N. Clayton (1972), Oxygen isotope studies of fresh and weathered submarine basalts, *Can. J. Earth Sci.*, *9*, 172–184.
Pichat, S., C. Douchet, and F. Albarède (2003), Zinc isotope variations in deep-sea carbonates from the Eastern Equatorial Pacific over the last 175 ka, *Earth Planet. Sci. Lett.*, *210*, 167–178.
Pons, M.-L., G. Quitté, T. Fujii, M. T. Rosing, B. Reynard, F. Moynier, C. Douchet, and F. Albarède (2011), Early Archean serpentine mud volcanoes at Isua, Greenland, as a niche for early life, *Proc. Natl. Acad. Sci. U.S.A.*, *108*, 17,639–17,643.
Pribil, M. J., R. B. Wanty, W. I. Ridley, and D. M. Borrok (2010), Influence of sulfur-bearing polyatomic species on high precision measurements of Cu isotopic composition, *Chem. Geol.*, *272*, 49–54.
Prytulak, J., S. G. Nielsen, D. A. Ionov, A. N. Halliday, J. Harvey, K. A. Kelley, Y. L. Niu, D. W. Peate, K. Shimizu, and K. W. W. Sims (2013), The stable vanadium isotope composition of the mantle and mafic lavas, *Earth Planet. Sci. Lett.*, *365*, 177–189.
Ripley, E. M., J. G. Brophy, and C. Li (2002), Copper solubility in a basaltic melt and sulfide liquid/silicate melt partition coefficients of Cu and Fe, *Geochim. Cosmochim. Acta*, *66*, 2791–2800.
Rouxel, O., N. Dobbek, J. Ludden, and Y. Fouquet (2003), Iron isotope fractionation during oceanic crust alteration, *Chem. Geol.*, *202*, 155–182.
Rouxel, O., Y. Fouquet, and J. N. Ludden (2004), Copper isotope systematics of the Lucky Strike, Rainbow, and Logatchev Sea-Floor hydrothermal fields on the Mid-Atlantic Ridge, *Econ. Geol.*, *99*, 585–600.
Savage, P. S., J. Wimpeny, J. Harvey, Q.-Z. Yin, and F. Moynier (2013), Investigating the effects of abyssal peridotite alteration on Si, Mg and Zn isotopes, AGU2013 Conference Abstracts V54A-06.
Savage, P. S., J. Harvey, and F. Moynier (2014), Copper isotope heterogeneity in the lithospheric mantle, Goldschmidt2014 Conference Abstracts 2192.
Savage, P. S., F. Moynier, H. Chen, G. Shofner, J. Siebert, J. Badro, and I. S. Puchtel (2015), Copper isotope evidence for large-scale sulphide fractionation during Earth's differentiation, *Geochem. Persp. Lett.*, *1*, 53–64.
Seewald, J. S., and W. E. Seyfried Jr. (1990), The effect of temperature on metal mobility in subseafloor hydrothermal systems: Constraints from basalt alteration experiments, *Earth Planet. Sci. Lett.*, *101*, 388–403.
Seo, J. H., S. K. Lee, and I. Lee (2007), Quantum chemical calculations of equilibrium copper (I) isotope fractionations in ore-forming fluids, *Chem. Geol.*, *243*, 225–237.
Sossi, P. A., G. P. Halverson, O. Nebel, and S. M. Eggins (2015), Combined separation of Cu, Fe and Zn from rock matrices and improved analytical protocols for stable isotope determination, *Geostand. Geoanal. Res.*, *39*, 129–149.
Sun, X., Q. Tang, W. Sun, L. Xu, W. Zhai, J. Liang, Y. Liang, K. Shen, Z. Zhang, and B. Zhou (2007), Monazite, iron oxide and barite exsolutions in apatite aggregates from CCSD drillhole eclogites and their geological implications, *Geochim. Cosmochim. Acta*, *71*, 2896–2905.
Staudigel, H., G. R. Davies, S. R. Hart, K. M. Marchant, and B. M. Smith (1995), Large scale isotopic Sr, Nd and O isotopic anatomy of altered oceanic crust: DSDP/ODP sites 417/418, *Earth Planet. Sci. Lett.*, *130*, 169–185.
Teagle, D. A. H., J. C. Alt, S. Umino, S. Miyashita, N. R. Banerjee, D. S. Wilson, and T. E. Scientists (2006), Superfast spreading rate crust, Proc. Integr. Ocean Drill. Program, 309/312.
Teagle, D. A. H., B. Ildefonse, P. Blum, and T. I. E. Scientists (2012), IODP Expedition 335: Deep sampling in ODP Hole 1256D, *Sci. Drilling*, *13*, 28–34.
Vance, D., C. Archer, J. Bermin, J. Perkins, P. J. Statham, M. C. Lohan, M. J. Ellwood, and R. A. Mills (2008), The copper isotope geochemistry of rivers and the oceans, *Earth Planet. Sci. Lett.*, *274*, 204–213.
Von Damm, K. L., J. M. Edmond, B. Grant, C. I. Measures, B. Walden, and R. F. Weiss (1985), Chemistry of submarine hydrothermal solutions at 21 °N, East Pacific Rise, *Geochim. Cosmochim. Acta*, *49*, 2197–2220.
Wall, A. J., R. Mathur, J. E. Post, and P. J. Heaney (2011), Cu isotope fractionation during bornite dissolution: An in situ X-ray diffraction analysis, *Ore Geol. Rev.*, *42*, 62–70.

Wilkinson, J. J., D. J. Weiss, T. F. D. Mason, and B. J. Coles (2005), Zinc isotope variation in hydrothermal systems: Preliminary evidence from the Irish Midlands Ore Field, *Econ. Geol.*, *100*, 583–590.

Wilson, D. S., D. A. H. Teagle, and G. D. Acton (2003), *Proceedings of the Ocean Drilling Program, Initial Reports*, vol. 206, Ocean Drill. Program, College Station, Tex.

Wilson, D. S., et al. (2006), Drilling to Gabbro in intact ocean crust, *Science*, *312*, 1016–1020.

Xu, Y.-G. (2014), Recycled oceanic crust in the source of 90–40 Ma basalts in North and Northeast China: Evidence, provenance and significance, *Geochim. Cosmochim. Acta*, *143*, 49–67.

Yang, W., F.-Z. Teng, H.-F. Zhang, and S. G. Li (2012), Magnesium isotopic systematics of continental basalts from the North China craton: Implications for tracing subducted carbonate in the mantle, *Chem. Geol.*, *328*(3–4), 185–194.

Zhu, X. K., et al. (2002), Mass fractionation processes of transition metal isotopes, *Earth Planet. Sci. Lett.*, *200*, 47–62.